Available online at www.sciencedirect.com
ScienceDirect
Cement & Concrete Composites 30 (2008) 745–761
Cement & Concrete Composites
www.elsevier.com/locate/cemconcomp

Load resistance of masonry wallettes and shear triplets retrofitted with GFRP composites

S. Suriya Prakash, P. Alagusundaramoorthy *

Structural Engineering Division, Indian Institute of Technology Madras, India

Received 12 October 2005; received in revised form 24 October 2007; accepted 9 November 2007
Available online 23 November 2007

Abstract

Masonry is one of the conventional materials that is being used throughout the world due to its accessibility, functionality and cost but they fail in earthquakes mainly due to their low tensile and shear resistance. The objective of this investigation is to study the effectiveness of GFRP composite retrofitting on the behaviour of masonry wallettes and shear triplets that are cast with low stiffness table moulded bricks and high stiffness cement mortar through experimental and finite element study. Experiments were conducted on masonry wallettes under compression in different orientations and triplets under shear. Finite element models for the analysis of wallettes and shear triplets is developed using the FE software ABAQUS and validated with the experimental data. The concepts of macromodeling with smeared crack concrete model for masonry wallettes and micromodeling with the elastic properties of brick and mortar for shear triplets are used for the analysis. The changes in deformational capacity and ultimate load resistance are calculated for varying thickness and fiber orientations of GFRP composites. Based on this study, it is concluded that the strength and axial stiffness of the wallettes under compression and strength of shear triplets is increased due to external bonding of GFRP composites. The comparison of finite element and experimental results proved that macromodeling can be used to study behaviour of masonry wallettes retrofitted with GFRP composites and micromodeling is feasible for the analysis of small scale specimens such as triplets.

Keywords: Masonry; Wallettes; Triplets; GFRP composites; Retrofitting; Macromodeling; Micromodeling

1. Introduction

The seismic behaviour of unreinforced masonry is brittle with a little or no ductility that leads to various damages ranging from invisible cracking to extensive crushing resulting in loss of life and property. The failure of masonry structures during earthquakes is found to be the main cause for the loss of life and serious injury [13]. The existing masonry buildings need to be rehabilitated/retrofitted to improve their seismic performance for reducing the catastrophic failures. The objective of the retrofitting is to enhance the earthquake resistance of masonry structures in order to avoid its failure in brittle manner. The usage of fiber reinforced polymers to enhance the seismic performance of masonry structures is a promising technique due to its high specific strength, high stiffness and small thickness compared to conventional materials [28]. Retrofitting of masonry walls with FRP composites has been found to produce remarkable increase in the inplane and out of plane strength [1,3,4,7,8,9,29,30]. However, all these studies were carried out on masonry assemblages with high stiffness bricks and low stiffness mortar. The effect of FRP retrofitting on the structural performance of masonry structures found in Indian subcontinent which are typically made of bricks with low stiffness and high stiffness mortar needs to be studied either through small-scale testing of masonry components such as wallettes and triplets or by full scale testing of retrofitted masonry walls. Small scale tests on FRP retrofitted masonry assemblages could reduce the time, labor and cost. The effect of different

* Corresponding author. Tel.: +91 44 22574276.
E-mail address: aspara0@iitm.ac.in (P. Alagusundaramoorthy).

0958-9465/$ - see front matter © 2007 Elsevier Ltd. All rights reserved.
doi:10.1016/j.cemconcomp.2007.11.005

Nomenclature

E_x	modulus of elasticity of masonry along the bed joints in N/mm^2	υ_{yx}	Poisson's ratio along yx-direction
E_y	modulus of elasticity of masonry normal to the bed joints in N/mm^2	E_{45}	modulus of elasticity along 45° direction in N/mm^2
E_b	modulus of elasticity of brick in N/mm^2	υ_{45}	Poisson's ratio in the 45° direction tension coupon
E_m	modulus of elasticity of mortar in N/mm^2	σ_u^c	ultimate uniaxial compressive strength
G_{xy}	shear modulus along the plane xy in N/mm^2	σ_1, σ_2	principal stresses in 1 and 2 directions
G_{xz}	shear modulus along the plane xz in N/mm^2	σ_r	fraction of remaining direct tensile stress
G_{yz}	shear modulus along the plane yz in N/mm^2	σ_{cr}	direct tensile stress at cracking
p	equivalent pressure stress	ξ	absolute value of the direct tensile strain
q	deviatoric stress	ξ_{cr}	direct tensile strain at cracking
υ_{xy}	Poisson's ratio along xy-direction	τ_{xy}	shear stresses in the xy-direction

variables like type of masonry, FRP composites and retrofitting configuration on the performance of retrofitted masonry can be studied in an economical way through tests on masonry assemblages like wallettes and shear triplets supplemented with full scale testing.

The evolution of finite element techniques has also made possible the more refined analysis of complex masonry structures retrofitted with FRP composites. Finite element modeling can provide an insight in to the structural behaviour of FRP retrofitted masonry and can support the derivation of rational design rules. However, only limited analytical studies are found in the literature on the effectiveness and reliability of FRP retrofitting on masonry structures [12,14,24,25] and this mainly due to the lack of accurate models to understand the complex behaviour of units, mortar joints and masonry as composite material retrofitted with FRP another composite material. The finite element models for masonry are categorized into homogeneous models such as macromodeling and heterogeneous models such as micromodeling. In homogeneous material modeling, the behaviour of masonry is modeled using a fictitious material having the material properties equivalent to the material behaviour of brick masonry [15,23]. In the heterogeneous modeling, the bricks and mortar are not only modeled separately through their respective constitutive law but their interaction between them is also considered [22,24,26]. Researchers have also adopted simplified macormodeling for analysis of masonry using homogenization procedures [21,14,24]. All the studies reported on the literature have investigated the behaviour of masonry structures with and without FRP retrofitting made of high stiffness bricks and low stiffness mortar.

At present, codal provisions are available for the masonry made with high stiffness brick with low stiffness mortar. Only limited data about the basic mechanical properties of masonry made of high stiffness mortar and low stiffness brick are available. The objective of the present study is to understand load resistance/deformation characteristics and failure modes of masonry wallettes and shear triplets made of low stiffness brick and high stiffness mortar through experimental and finite element study. This study mainly focused on the generation of data about the mechanical properties and failure modes of masonry with high stiffness bricks with low stiffness mortar and validation of the results using existing finite element modeling techniques. The validated FE models can be used for parametric study and development of codal provisions. Tests on GFRP retrofitted wallettes and shear triplets are oriented towards establishing simple constitutive models for design and strength evaluation of FRP upgraded walls.

2. Experimental study

The basic material properties of masonry components are essential to understand the behaviour of FRP composite retrofitted masonry through experimental and finite element study. The strength and elastic properties of bricks, cement mortar, brick masonry wallettes, brick masonry shear triplets and GFRP composite materials were evaluated through testing. The test specimens and test setup are shown in the Fig. 1.

2.1. Characterization of resin and GFRP composites

Glass fiber woven roving mat with epoxy resin were used for retrofitting in this study. The strength of GFRP composite depends on the mechanical properties of its constituents namely epoxy resin and woven roving mat. The material properties of resin such as viscosity, gel time, peak exothermic temperature, tensile strength and flexural strength plays an important role in the effective utilization of GFRP composites. Low tensile strength of epoxy resin may lead to cracking of resin and that results in premature debonding of GFRP composites and hence the characterization of resin and GFRP composite materials is essential. Tests were conducted on epoxy resin to find the specific gravity, viscosity, gel time and peak exotherm, tensile strength, flexural strength and heat deflection temperature

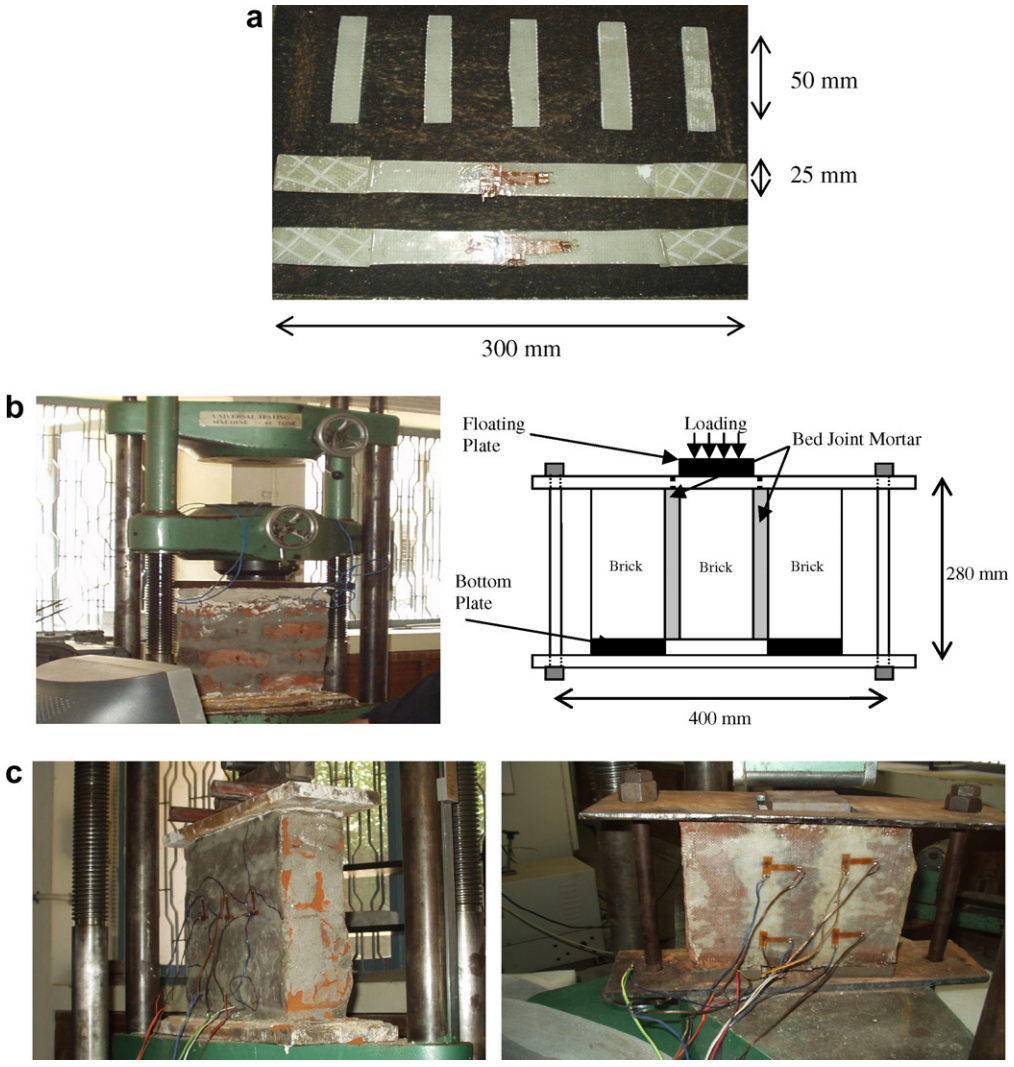

Fig. 1. (a) GFRP composite coupons, (b) wallette and shear triplet specimens and (c) retrofitted wallette and shear triplet specimens.

as per BS 2782-10:1996 [5]. Tests were conducted on GFRP composites consisting of six layers of glass fiber woven roving mat (WRM) of 360 grams per meter square (gsm) and epoxy resin with fiber to resin ratio as 1:1 to find the water absorption, hardness, volume fraction of fibers, tensile strength and flexural strength. Six layers of reinforcement were used in order to achieve a minimum thickness of 3 mm for the flexural test. The properties of resin and GFRP composites used for the retrofitting are given in Table 1.

2.2. Tests on clay bricks and mortar

The clay bricks were tested under uniaxial compression to find the material parameters such as modulus of elasticity and compressive strength. Six bricks were tested with the average size of 220 mm × 110 mm × 70 mm. The bed faces of brick were capped using a rich cement mortar of 1:2 and completely saturated in water for two days as per IS: 3495-1976 [19] and subjected to uniform compressive loading in a compression testing machine. The top capped surfaces were covered by plaster of Paris and plywood to apply uniform pressure. The capped specimens were tested under load control in the universal testing machine. The loading rate was adjusted such that the test was completed in not less than 1 min and not more than 2 min. The average modulus of elasticity of the bricks was calculated as 808 N/mm^2 from the test results (Table 2). The compression test results on bricks showed wide variation in strength and stiffness. The average compressive strength of bricks under compression normal and parallel to bed joint was respectively 9.6 N/mm^2 and 4.3 N/mm^2. These wide variations can be attributed to their inherent nature of manufacturing process. Mortar cubes of size 70 mm × 70 mm × 70 mm were cast with cement sand in the ratio of 1:5 for M1 grade with a minimum compressive strength of 5 N/mm^2 and tested at 3 days, 7 days and 28 days as per IS: 1905-1987 [20] to find the material parameters. The mortar cubes were tested under load control in the universal testing machine. The loading rate was adjusted such that the

Table 1
Properties of resin and GFRP composites

S. no.	GFRP composites		Epoxy resin	
	Property	Value	Property	Value
1	Water absorption	0.04%	Specific gravity	1.164
2	Barcol hardness	46	Viscosity	4180 cP
3	Volume fraction of fiber by weight	0.43	Gel time	23 min
4	Volume fraction of resin by weight	0.57	Peak exotherm	167 °C
5	Flexural strength	310 N/mm^2	Heat deflection temperature	126 °C
6	Flexural modulus	10,260 N/mm^2	Tensile strength	53 N/mm^2
7	Tensile strength for 0° angle ply	121 N/mm^2	Tensile modulus	1634 N/mm^2
8	Tensile modulus for 0° angle ply	11,500 N/mm^2	Flexural strength	148 N/mm^2
9	Tensile strength for 90° angle ply	126 N/mm^2	Flexural modulus	5284 N/mm^2
10	Tensile modulus for 90° angle ply	12,986 N/mm^2	–	–
11	Tensile strength for 45° angle ply	180 N/mm^2	–	–
12	Tensile modulus for 45° angle ply	10,704 N/mm^2	–	–
13	Shear modulus	3740 N/mm^2	–	–
14	Major Poisson's ratio (υ_{xy})	0.126	–	–
15	Minor Poisson's ratio (υ_{yx})	0.112	–	–

Table 2
Ultimate strength of bricks under compression

Specimen number	Failure load (kN)	Ultimate stress (N/mm^2)	Ultimate strain	Young's modulus (N/mm^2)
1	240	9.9	Strain readings were not consistent	Strain readings were not consistent
2	230	9.5	Strain readings were not consistent	Strain readings were not consistent
3	250	10.3	Strain readings were not consistent	Strain readings were not consistent
4	210	8.7	Strain readings were not consistent	Strain readings were not consistent
5	255	10.5	0.013	807
6	230	9.5	0.012	791
7	220	9.1	0.011	827
Average	234	9.6	0.012	808

test was completed in not less than 1 min and not more than 2 min. The details of the test results are shown in the Table 3. The average modulus of elasticity of the mortar cube was calculated as 1540 N/mm^2 from the test results. The modulus of elasticity of the cement mortar was found to be 90% higher than that of brick under compression. This is unlike the case of brick masonry in North America, Canada and Europe where high elastic modulus brick units are used in combination with mortar of low elastic modulus.

2.3. Tests on masonry wallettes

The masonry wallettes were made with bricks using cement mortar of 1:5 with a height to length ratio equal to one and height to thickness ratio equal to three (Table 4) as per IS: 1905-1987[20] and EN 1052-1[11]. The average size of brick masonry wallettes was 407 mm × 395 mm × 126 mm. Nine masonry wallettes were cast and used as control specimens. Five specimens such as WNB1–WNB5 were tested under compression normal to bed joints and the remaining four namely WPB6–WPB9 were tested under compression parallel to bed joints. The wallettes were cured for 15 days and tested in compression testing machine under displacement control. The load was applied at the rate of 0.01 mm/s. To ensure uniform pressure, 20 mm thick steel plates with plaster of Paris are placed on the top and bottom of the wallettes. The strain along the axis of the loading and in the transverse directions was measured using demec gauges with a gauge length of 200 mm. The orthotropic properties of masonry were obtained through compression tests on wallettes with loading normal and parallel to bed joints (Fig. 2).

Table 3
Compressive strength of mortar

Number of specimens	Number of days of curing	Average weight of the cube (N)	Average failure load (kN)	Average ultimate stress (N/mm^2)	Average Young's modulus (N/mm^2)
3	3	7.40	10	2.0	–
3	7	7.50	20	4.1	–
3	28	7.56	35	7.1	1540 N/mm^2

2.3.1. Control unretrofitted wallettes

The control specimens under uniaxial compression test normal to bed joint (WNB1–WNB5) failed through vertical cracking in the middle of wallettes (Fig. 2a). Under uniaxial compression, the low stiffness brick tends to expand laterally faster than high stiffness mortar. But the mortar

Table 4
Ultimate strength of wallettes under compression

Specimen	Direction of loading	Size ($l \times b \times t$) (mm)	Density (kN/m^3)	Ultimate strength (N/mm^2)	Ultimate strain	Young's modulus (N/mm^2)	Axial secant stiffness at failure (AE/l) (kN/mm)
WNB1	Normal to bed joint	393 × 410 × 132	19,600	3.3	Strain readings were not consistent	Strain readings were not consistent	Strain readings were not consistent
WNB2	Normal to bed joint	395 × 410 × 130	19,400	2.6	Strain readings were not consistent	Strain readings were not consistent	Strain readings were not consistent
WNB3	Normal to bed joint	396 × 405 × 122	19,300	3.3	0.01900	176	21.97
WNB4	Normal to bed joint	398 × 408 × 126	19,600	3.1	0.01920	163	21.1
WNB5	Normal to bed joint	390 × 404 × 123	19,500	3.0	0.01850	164	20.9
Average		395 × 407 × 126	19,520	3.0	0.01890	168	21.3
WPB6	Parallel to bed joint	392 × 408 × 123	19,900	3.3	0.00775	425	54.4
WPB7	Parallel to bed joint	396 × 409 × 125	20,800	3.2	0.00765	420	54.2
WPB8	Parallel to bed joint	398 × 406 × 127	19,600	3.0	0.00770	393	50.9
WPB9	Parallel to bed joint	393 × 408 × 128	21,200	2.9	0.00775	381	50.6
Average		396 × 407 × 127	20,375	3.1	0.00771	405	52.6
RWNB1	Normal to bed joint	395 × 408 × 130	20,400	3.6	0.01140	316	42.4
RWNB2	Normal to bed joint	396 × 406 × 131	20,600	3.9	0.01120	348	46.8
RWNB3	Normal to bed joint	396 × 405 × 128	20,500	4.1	0.01190	345	45.2
Average		396 × 406 × 130	20,500	3.9	0.01150	336	44.8
RWPB4	Parallel to bed joint	394 × 409 × 130	20,300	3.5	0.00580	603	81.4
RWPB5	Parallel to bed joint	397 × 407 × 129	20,800	3.2	0.00570	561	74.2
RWPB6	Parallel to bed joint	396 × 406 × 128	20,200	3.0	0.00570	526	69.1
Average		396 × 406 × 129	20,433	3.2	0.00570	563	74.9

prevents this lateral expansion and it creates a stress state of triaxial compression in bricks thereby resulting tensile stresses in the mortar. As soon as the principal tensile stress reaches the tensile strength of the mortar, crack forms and the failure occur. The same size of wallettes that were cast for the testing under uniaxial compression normal to bed joint were cast and tested under compression parallel to the bed joint. The specimens under compression parallel to bed joint (WPB6–WPB9) failed by the formation of vertical cracks along the bed joint mortar due to differential normal deformation of bricks and the mortar joint (Fig. 2b). The ultimate strength, failure strain and Young's modulus obtained from the tests are shown in Table 4. The average modulus of elasticity was found to be 168 N/mm^2. The modulus of elasticity of wallettes along parallel to bed joint was calculated as 405 N/mm^2. The low modulus of elasticity of masonry is mainly due to the low strength of bricks which were procured from the local suppliers. Low modulus of elasticity of wallettes in the range of 262–735 N/mm^2 under compression is also reported in the literature [16]. The ultimate compressive strain of wallettes under compression parallel to bed joint is lower than that of normal to the bed joint due to the sudden splitting failure with formation of full length crack along the bed joint. The modulus of elasticity of wallettes under compression parallel to bed joint was higher than the modulus of elasticity normal to bed joint (Table 4).

2.3.2. GFRP composite retrofitted wallettes

Six masonry wallettes such as RWNB1–RWPB6 were cast and retrofitted with two layers of GFRP composites of 0.86 mm thickness. The wet lay-up technique was adopted to bond the glass fiber fabric on the masonry

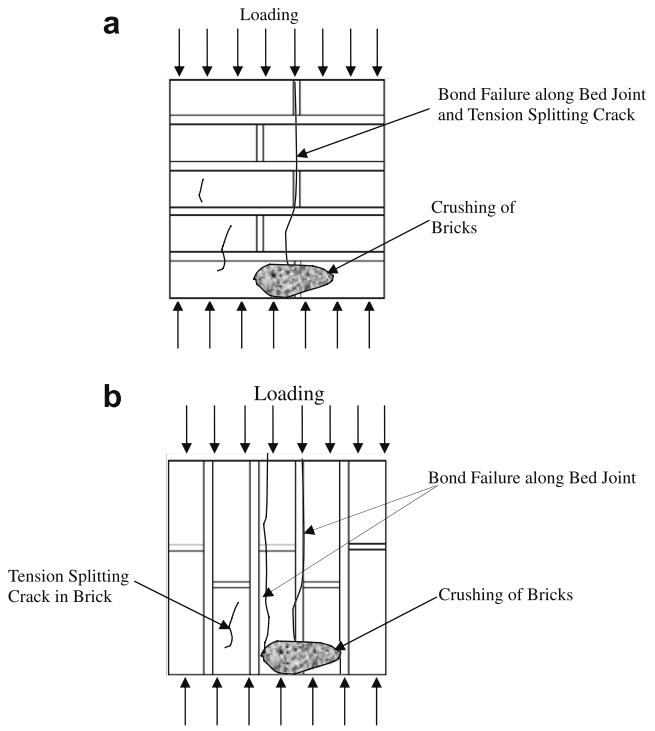

Fig. 2. Failure mode of the wallettes under compression: (a) loading normal to bed joints and (b) parallel to bed joints.

wallette surface. The presence of any moisture would affect the laying of GFRP composite and its performance very severely hence the specimen was dried completely for 7 days after curing for 15 days. It was taken care to remove the loose particles and excessive mortar from the mortar joint, since the bonding of GFRP composites with the mortar joint plays a major role in increasing the strength and deformational capacity. Epoxy resin of LY556 with the hardener of HY951 mixed in the ratio of 1:0.1 by weight was used as the resin system. Two layers of glass fiber fabric of WRM 360 gsm, compatible with epoxy resin was used as reinforcement. Glass fiber fabric of required quantity was calculated based on the surface area to be retrofitted. The face of masonry surface was made rough to a coarse sand paper texture by scarifying before applying the thoroughly mixed resin system. A thick layer of two-component saturating epoxy was applied on the masonry surface using a paint roller. The bonding surface of the glass fiber woven roving mat was then cleaned with acetone. The woven roving mat was rolled on the masonry surface and pressed into place at the center and moved towards top and bottom of the wallette. The woven roving mat was kept tight and wrinkles free. A thick layer of saturating epoxy was then applied on the glass fiber fabric. Another layer of woven roving mat was applied and the total thickness of the retrofitting GFRP composite was 0.86 mm. Entrapped excessive air was removed from the surface by careful rolling of the paint rollers. It was taken care to maintain the same volume fraction of fibers while retrofitting as in the case of coupon tests.

GFRP retrofitting (RWNB1–RWNB3) increased the ultimate load resistance of wallettes under compression normal to bed joint significantly compared to WNB1–WNB5. The average increase in the load resistance due to GFRP retrofitting was up to 20% but the average ultimate strain reduced significantly up to 40% due to GFRP retrofitting which is detrimental to the seismic demand (deformational capacity). It should be noted that test specimens were not intended to take full advantage of the confinement mechanism of GFRP composite and its buckling resistance. The objective is to suggest simple constitutive models and to validate the effectiveness of GFRP composite retrofitting. The average axial secant stiffness at the failure of the retrofitted specimen is $AE/l = 44.7$ kN/mm compared to the control specimen axial secant stiffness at failure of $AE/l = 21.3$ kN/mm (Table 4) and the increase in axial secant stiffness of the wallettes due to retrofitting was up to 110%. The applied axial compression load was resisted by the composite section consisting of thickness of masonry wallette and GFRP composite till from the beginning of loading. The same amount of increase in stiffness was observed in all the three tested specimens till from the beginning of loading. The increase in stiffness is due to the overlap of GFRP composite to the top surface of wallette by about 20 mm while retrofitting on each side. This resulted in a coverage of 60% of the cross sectional area of the wallettes. The increase in stiffness could also be attributed to partial confinement of the laminates. Rule of mixtures, also indicates the same. By rule of mixtures:

$$\begin{aligned}\text{Stiffness}_{(\text{retrofitted})} &= E \times \text{Thickness}_{(\text{masonry})} \\ &\quad + E_{\text{GFRP}} \times \text{Thickness(GFRP)} \\ \text{Stiffness}_{(\text{retrofitted})} &= 168 \times 70 + 11,500 \times (2 \times 0.86) \\ &= 31,540 \text{ N/mm} \\ \text{Stiffness}_{(\text{unretrofitted})} &= 168 \times 70 = 11,760 \text{ N/mm} \\ \text{Increase in stiffness} &= \frac{31,540 - 11,760}{11,760} = 1.682\end{aligned}$$

This shows the possibility of more than 100% increase in stiffness. This amount of increase seems to be very high owing to the very low stiffness of masonry considered in the study. The retrofitted wallettes failed under compression by crushing due to the confining effect of retrofitted laminates. A bursting sound was heard while reaching the ultimate load and the load shedding took place immediately. The test was stopped at 50% of the ultimate load resistance. Although the debonding sound of the laminates was heard at the initial phase of loading, the overall bond between GFRP and brick surface was intact throughout the loading (Fig. 3a).

GFRP retrofitting (RWPB4–RWPB6) increased the ultimate load resistance of wallettes under compression parallel to bed joint compared to WPB6–WPB9. The average increase in the load resistance due to GFRP retrofitting was up to 5% but the average ultimate strain reduced up to 26%. The average axial secant stiffness at failure of the

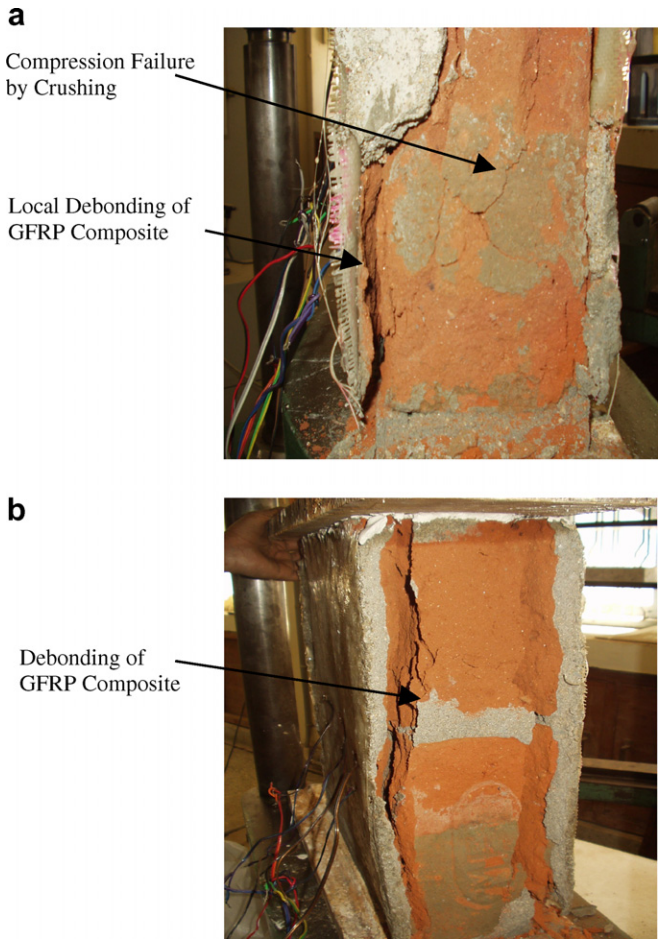

Fig. 3. Failure modes of the wallettes under compression: (a) loading normal to bed joints and (b) parallel to bed joints.

retrofitted specimen is $AE/l = 74.9$ N/mm compared to the control specimen of $AE/l = 52.5$ N/mm (Table 4) and the increase in the axial stiffness due to retrofitting is up to 43%. The increase in stiffness is due to the overlap of laminates which resulted in the partial confinement of the laminates. A bursting sound was heard while reaching the peak load as a result of separation of the GFRP fabric from the bricks. The gradual debonding of GFRP laminates resulted in gradual decrease in the load resistance unlike under compression normal to bed joint. The overall bond was intact even up to failure though there was local debonding along the bed joint mortar. The failure mode of the wallette under compression parallel to bed joints is shown in the Fig. 3b. The test was stopped as soon as the load resistance dropped up to 50% of the ultimate load.

2.4. Tests on shear triplets

Six shear triplet specimens were cast with the average size of $230 \times 233 \times 110$ mm. Three specimens namely STS1–STS3 were tested as control unretrofitted specimens. Three specimens RSTS1–RSTS3 were retrofitted with a layer of GFRP composite of thickness 0.43 mm by wet lay up process as discussed in Section 2.3.2 and tested under static loading.

2.4.1. Control unretrofitted shear triplets

Three shear triplet specimens (STS1–STS3) were cast with the average size of $230 \times 233 \times 110$ mm. The specimens were tested under zero vertical compression normal to bed joint with displacement control compression testing machine to determine the initial shear strength of brick masonry as per EN 1052-1 [11]. A test setup was fabricated for testing the shear triplet specimens. It consists of top and bottom steel plates connected by bolts at the ends (Fig. 4a). A slot was provided in the top plate to accommodate the floating plate. The pure shear loading was applied exactly at the middle brick in the triplet through the floating plate at the slot of the top plate. The rate of loading was kept as 0.001 mm/s. The shear resistance increased without deformation up to a load of 10 kN and increased linearly from 10 kN to 14 kN up to a deformation of 0.01 mm. The load resistance was constant between 0.01 mm and 0.02 mm. The crack started propagating along the bed joint after a deformation of 0.02 mm and the specimen failed suddenly (Fig. 4a). This showed that the triplets without retrofitting failed through splitting of brick and bed joint mortar at very low displacement. This is a result of the weak mortar joint bond strength and the absence of friction resistance due to the lack of compressive stress normal to bed joints. Similar failure mode was also reported by Hamid et al. [17]. The average ultimate shear strength between the brick and mortar layer and the deformation of shear triplets was found to be 0.29 N/mm^2 and 0.018 mm, respectively. The test results of unretrofitted shear triplets are given in the Table 5.

2.4.2. GFRP composite retrofitted shear triplets

The GFRP composite retrofitted shear triplet was tested under pure shear loading. Although there was some initial debonding observed along the bed joint, the final failure of the shear triplet was by cracking of the middle brick (Fig. 4b). Similar mode of failure was also reported by Hamid et al. [17]. This failure mode implies that the shear failure can be eliminated by GFRP retrofitting and the strength will be governed by compressive strength only. The GFRP retrofitting increased the ultimate load of shear triplets (RSTS) from 13.8 kN to 39 kN. The test results of retrofitted shear triplets (RSTS) are given in the Table 5. The GFRP retrofitting increased the ultimate displacement from 0.018 mm to 2.967 mm (Table 5) and the increase in the ultimate load resistance was up to 180%. This showed that the deformational capacity and the load resistance of the masonry under shear were increased by GFRP composite retrofitting.

3. Finite element study

Smeared crack concrete model [18] can be used to predict the behaviour under monotonic loading for brittle

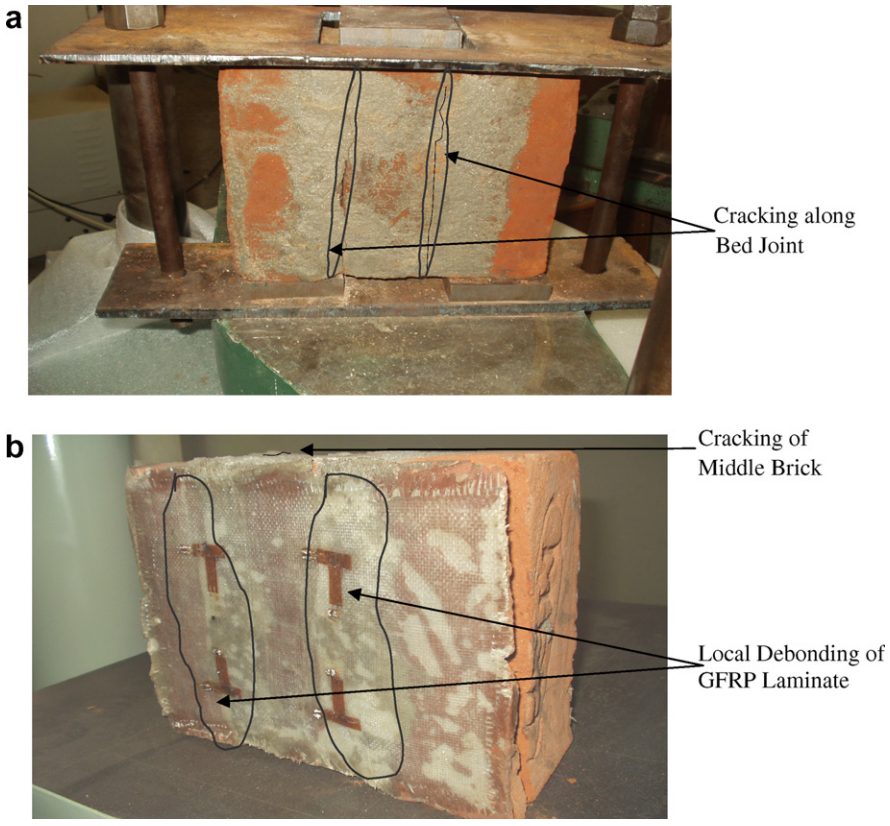

Fig. 4. Failure mode of shear triplets: (a) control specimen (STS) and (b) retrofitted specimen (RSTS).

Table 5
Ultimate shear strength of control and retrofitted triplets

Specimen	Size ($l \times b \times h$) (mm)	Failure load (kN)	Ultimate shear strength (N/mm^2)	Maximum shear deformation (mm)
STS1	233 × 110 × 230	13.5	0.28	0.020
STS2	232 × 110 × 230	14.2	0.29	0.020
STS3	233 × 110 × 230	13.9	0.29	0.014
Average	233 × 110 × 230	13.8	0.29	0.018
RSTS1	234 × 112 × 230	37.8	0.78	3.200
RSTS2	232 × 112 × 230	39.3	0.81	2.900
RSTS3	232 × 112 × 230	40.0	0.83	2.800
Average	233 × 112 × 230	39.0	0.81	2.967

materials like masonry that exhibits different yield strength along compression and tension. In macromodeling, the brick unit, mortar and interface are modeled using a single equivalent continuum. The advantage of using macromodeling is enormous reduction in computational cost and the analysis of large structures is possible. In smeared crack concrete model, the concept of oriented damaged elasticity (smeared cracking) with isotropic compressive plasticity representing the inelastic behaviour of masonry is used. It is defined using the uniaxial stress strain relations (Fig. 5a), tension stiffening data (Fig. 5b) from the uniaxial tension test results and optionally by defining the shear retention and the failure ratios options (Fig. 5c). The model consists of an isotropically hardening yield surface that is active when the stress is dominantly compressive and an independent "crack detection surface" that determines if a point fails by cracking (Fig. 5d). The smeared crack concrete model requires the uniaxial stress–strain relationship for the masonry and its post cracking behaviour under tension which is defined by the "tension stiffening" option. Even though tension stiffening option is inappropriate for the unreinforced masonry due to the lack of reinforcement default values for masonry were adopted to avoid the numerical instability problems. The failure surface for the masonry was defined using the appropriate values from the test results of Dhanasekar et al. [6] and Andreaus [2].

In micromodeling of shear triplets, the bricks and mortar are modeled separately through their respective constitutive law considering their interaction in between them. The primary aim of micromodeling is to represent the

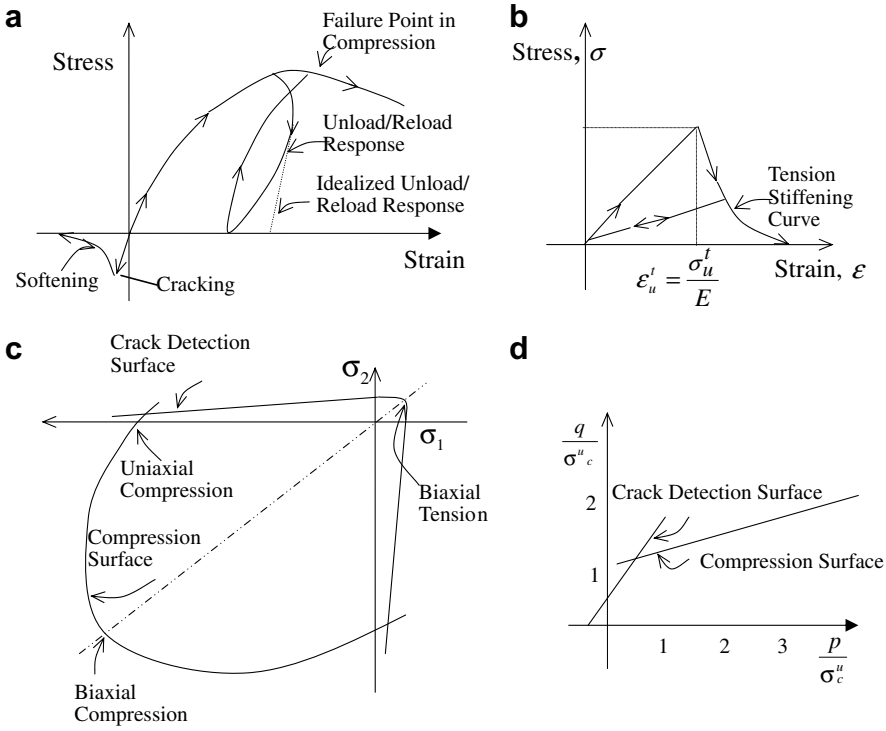

Fig. 5. Macro model for masonry wallettes: (a) uniaxial stress–strain relationship, (b) failure surface in P–Q stress space, (c) failure stress space in plane stress case and (d) tension stiffening data.

behaviour of masonry from the knowledge of constituent properties and the interface. The micromodeling strategy is particularly suited for the small structures and structural details where the interaction between the units and mortar is of prime interest since the mortar joint interfaces are the weakest element in the unreinforced masonry structures [10]. Micormodeling of real structures are difficult due to numerical convergence and heavy computational cost involved. Therefore, the concept of micromodeling is adopted for the analysis of masonry shear triplets. The micromodeling of masonry shear triplets helps to understand the behaviour and shear transfer mechanism through the mortar joint. The mechanism of shear transfer at a joint can be isolated into sliding, interlocking, overriding and fracture. Tests were conducted on shear triplet specimens (STS) under no vertical compression to find the shear strength of the brick masonry. The behaviour of three shear triplet specimens retrofitted with GFRP composites (RSTS) was also studied (Section 2.4, Table 5). The test results of the retrofitted triplets were used to validate the micromodel. In the present investigation, for the micromodeling of shear triplets the brick as well as mortar were taken as linear elastic materials with appropriate properties from the experimental data (Section 2.4, Table 6).

3.1. Material properties

The material properties for micromodeling were arrived by compression tests on bricks and mortar cubes were carried out as per IS 3495:1992 [19]. The average Young's modulus of the clay brick (E_b) masonry unit was found to be 808 N/mm^2 and the Poisson's ratio was taken as 0.2 (Table 2). The Young's modulus of the mortar (E_m) was found to be 1540 N/mm^2 and the Poisson's ratio was taken as 0.2 (Table 3). The friction in the interface between brick and mortar normally varies from 0.45 to 0.80 [27] and was taken as 0.6. The normal stiffness for the contact analysis was given very high value to avoid interpenetration of continuum. The material properties for macromodeling were obtained from the test results of brick masonry wallettes (Table 4). The average Young's modulus for the numerical study was calculated from the test data as 168 N/mm^2 normal to bed joint and 420 N/mm^2 parallel to bed joint. The Poisson's ratio for the brick masonry is between 0.15 and 0.2 and 0.2 is taken for the modeling. The low modulus of elasticity of masonry is mainly due to the low strength of bricks which were procured from the local suppliers. Low modulus of elasticity of wallettes in the range of

Table 6
Input parameters for the nonlinear part of macromodeling

Compression normal to bed joint		Compression parallel to bed joint	
Stress (N/mm^2)	Absolute plastic strain	Stress (N/mm^2)	Absolute plastic strain
3.10	0.00000	3.10	0.00000
3.00	0.00025	2.95	0.00170
2.90	0.00050	2.51	0.00355
2.50	0.00150	2.00	0.00515
1.60	0.00350	1.61	0.00675

262–735 N/mm^2 under compression normal to bed joint are also reported in the literature [16]. The tensile strength, flexural strength, water absorption, hardness and volume fraction of fibers of GFRP composites were obtained from testing (Section 2.1, Table 1). The average Young's modulus in tension along the warp and weft directions for the GFRP composite was found to be $E_x = 12{,}986$ N/mm^2 and $E_y = 11{,}500$ N/mm^2, respectively (Table 1). The major and minor Poisson's ratios υ_{xy} and υ_{yx} were found to be 0.126 and 0.112, respectively. The shear modulus was calculated from the 45° test coupon as $G_{xy} = G_{xz} = G_{yz} = E_{45}/2(1 + \upsilon_{45}) = 10{,}700/2(1 + 0.43) = 3740$ N/mm^2. The low tensile modulus and strength of GFRP composite is due to (i) the laminate was made by hand lay-up process with weight fraction of fibers of 0.43 only and (ii) commercially available woven roving mat (WRM) in India of 360 gsm was used. The biaxial state of stress is accounted for in the analysis using biaxial strength failure criterion. Tsai-Wu theory is used with material properties namely (i) tensile stress limit in the fiber direction (X_t), (ii) compressive stress limit in the fiber direction (X_c), (iii) tensile stress limit in the transverse direction (Y_t), (iv) compressive stress limit in the transverse direction (Y_c), shear strength (S), cross product term coefficient. The Tsai–Wu failure criterion option is included in the failure criterion option in ABAQUS as follows:

$$F_1\sigma_{11} + F_2\sigma_{22} + F_{11}\sigma_{11}^2 + F_{22}\sigma_{22}^2 + F_{66}\sigma_{12}^2 + 2F_{12}\sigma_{11}\sigma_{22} < 1.0$$

where

$$F_1 = \frac{1}{X_t} + \frac{1}{X_c}; \quad F_2 = \frac{1}{Y_t} + \frac{1}{Y_c}; \quad F_{11} = -\frac{1}{X_t \times X_c};$$
$$F_{22} = -\frac{1}{Y_t \times Y_c}; \quad F_{66} = -\frac{1}{S^2}; \quad F_{12} = -\frac{1}{2}\sqrt{f_{11} \times f_{22}}$$

However, the strains observed during the experiment and finite element study indicated that the strains in the laminate were well within the failure strains.

The parameters for the plastic part of the macromodel were taken from the nonlinear part of uniaxial compression stress strain curve (stress and corresponding absolute plastic strain) as given in Table 6. Tension stiffening data is the post cracking behaviour under uniaxial tension. The parameters of input for tension stiffening data are fraction of remaining stress to stress at cracking and the corresponding absolute value of the direct strain minus the direct strain at cracking. Default values such as if $\sigma_r/\sigma_{cr} = 1$, then ξ–$\xi_{cr} = 0$ and if $\sigma_r/\sigma_{cr} = 0$, then $\xi - \xi_{cr} = 0.006$ were assumed. The failure surface option was used to define the shape of the failure surface. The following four values were adopted to define failure surface for the masonry such as (i) the ratio of the ultimate biaxial compressive stress to the ultimate uniaxial compressive stress as 1.16, (ii) the absolute value of the ratio of the uniaxial tensile stress at failure to the ultimate uniaxial compressive stress as 0.09, (iii) the ratio of the magnitude of a principal component of plastic strain at ultimate stress in biaxial compression to the plastic strain at ultimate stress in uniaxial compression as 1.28 and (iv) the ratio of the tensile principal stress at cracking inplane stress, when the other principal stress is at the ultimate compressive value, to the tensile cracking stress under uniaxial tension as 0.33.

3.2. Discretization of wallettes and shear triplets

In the retrofitted and unretrofitted specimens, wallettes were modeled using eight noded linear continuum elements (C3D8R) with three translational degrees of freedom at each node with reduced integration and hourglass control. The GFRP composite fabric/sheet was modeled using 3D shell elements (S4R) having three rotations and three translations at each node. The mismatch in the degrees of freedom between shell and solid element is reconciled by coupling the degrees of freedom of solid elements to shell elements. Convergence study was carried out for all the developed FE models. The objective of the convergence study was to predict the maximum post peak response (i.e., maximum deformation till failure). Different mesh sizes were used for wallettes to predict the maximum post peak response. Coarser meshes with element size in the order of 30–50 mm resulted in the better prediction of post peak response. In micromodeling of shear triplets, both the brick and mortar was modeled using eight noded 3D continuum elements with three translation and rotational degrees of freedom at each node with hour glass control and reduced integration. The GFRP material was modeled using four noded 3D shell elements with three translational and rotational degrees of freedom and orthotropic material properties as in the case of retrofitted wallettes (Table 1).

3.3. Loading and boundary conditions

The nature and the speed of loading are important in performing nonlinear contact analysis. This is because the ultimate strength and mode of strength degradation is not known until the analysis ends. The incremental load was applied at the top surface of the wallette as displacement. The incremental load value was determined automatically at every loading step by arc-length control scheme built in ABAQUS. The bottom of the wallette was assumed to be fixed with all the degrees of freedom arrested. The analysis was carried out by applying the gravity loads in a stepwise fashion. The step by step analysis was carried out using a force based convergence criterion until the failure of most of the elements due to cracking/crushing that led to deterioration of stiffness matrix and the procedure became unstable. The geometry and loading conditions for the wallette are shown in the Fig. 6a. Perfect bond was assumed to exist between the wallette surface and GFRP composite. The assumption of the perfect bonding between the masonry and FRP sheets in strict sense is not valid when the damage starts occurring in the masonry. But, the experimental results of GFRP retrofitted wallettes and shear triplets showed

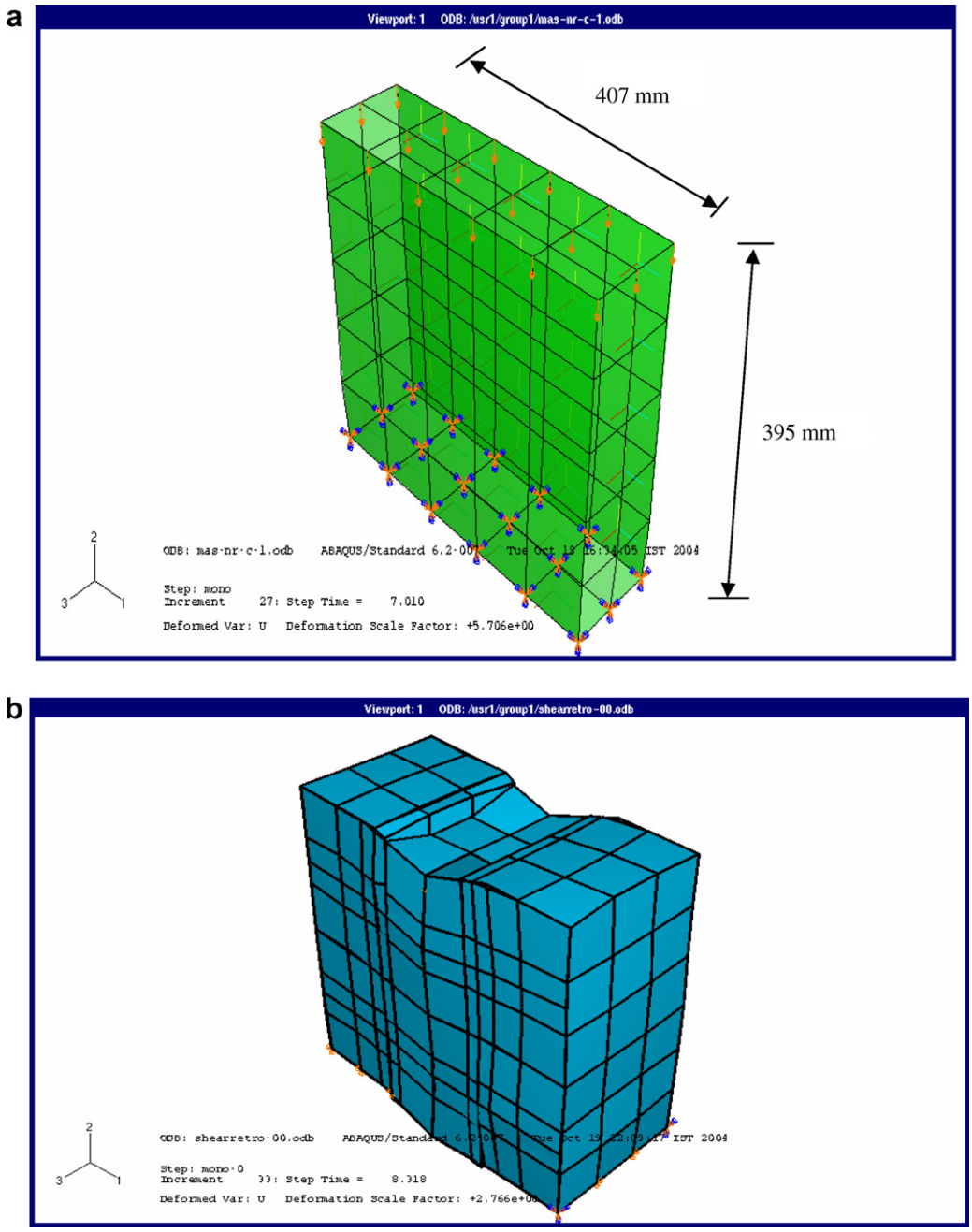

Fig. 6. Geometry and boundary conditions: (a) wallette model and (b) shear triplet.

that the retrofitted specimens failed mainly by compression rather than debonding. The overall bonding between masonry surface and GFRP composite was intact even at ultimate state though there was local debonding at few places. Based on this observation, perfect bonding was assumed to exist in order to make the model simple and computationally stable. In the micromodel of shear triplets, the incremental compressive load was applied at the top surface of the middle brick on the shear triplet in terms of displacement. The bottom of the side bricks were assumed to be fixed with all the degrees of freedom arrested. The interface between brick and mortar was modeled using surface to surface contact algorithm. The mortar surface was considered as master surface due to its higher modulus of elasticity and brick surface was considered as a slave surface. Tangential behaviour of the interface between the brick and mortar was modeled using penalty friction formulation using friction coefficient as 0.6. The normal behaviour of the interface was modeled using linear pressure on closure with normal stiffness as 1000 N/mm. The initial shear strength between the brick and mortar was simulated by giving a precompression of 0.29 N/mm^2. The geometry of the triplet and loading conditions are shown in the Fig. 6b.

3.4. Load deformation behaviour

The behaviour of the FE model was in close agreement with the experimental data up to the elastic limit in control wallette specimens (Fig. 7) and GFRP retrofitted wallettes (Fig. 8) under compression in the direction normal and parallel to bed joints. But the descending portion of the curves was unable to model and trace due to convergence difficulties. There was significant residual stress observed around the cracked elements along this portion. Adopting a discrete model can overcome this problem. Even with discrete crack approach, more computational effort is required to predict the post peak response. Convergence was also not found to be improved when mesh density of the wallettes were refined. This could also be attributed to the limitation of the smeared crack concrete model to predict the nonlinear behaviour in case of the small size wallettes where there is large confining pressure under axial compression. However, the smeared crack concrete model was found to predict the nonlinear behaviour reasonably well in the full-scale analysis of walls [13]. Through proper techniques by including the initial existing cracks should improve the convergence and this could be the scope for further research. The load resistance-displacement behaviour of GFRP retrofitted shear triplet was non linear as per the experimental data. The load resistance was constant initially before the cracking of the bed joint till 12 kN as in the case of control triplet (Fig. 9). After cracking through the bed joint, the GFRP started to resist the load. The ultimate strength of masonry will be governed by the compressive strength of masonry if the shear failure is eliminated. The ultimate load resistance from the finite element model was found to be 70 kN compared to the experimental value of 39 kN at the ultimate displacement of 3.0 mm (Fig. 9). This is due to the perfect bond assumption made in the modeling between the triplet surface and the GFRP surface neglecting the local debonding along the bed joint mortar. The non-linear shear behaviour of shear triplets is mainly due to the surface interaction of brick and mortar. The compressive stress distribution on the retrofitted wallette specimen is shown in the Fig. 10a. The shear stress (τ_{xy}) concentrations at the interface were reduced due to GFRP retrofitting. The shear stress distribution (τ_{xy}) at the brick mortar interface of GFRP retrofitted triplet is shown in the Fig. 10b. This shows that the shear failure of masonry can be eliminated through retrofitting with GFRP composites.

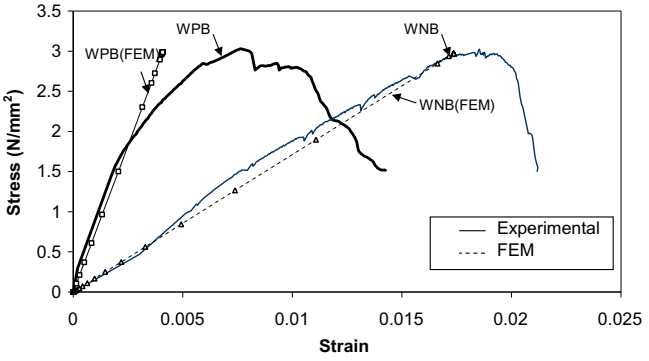

Fig. 7. Comparison of Fe result with experimental data for control wallette specimens normal and parallel to bed joint.

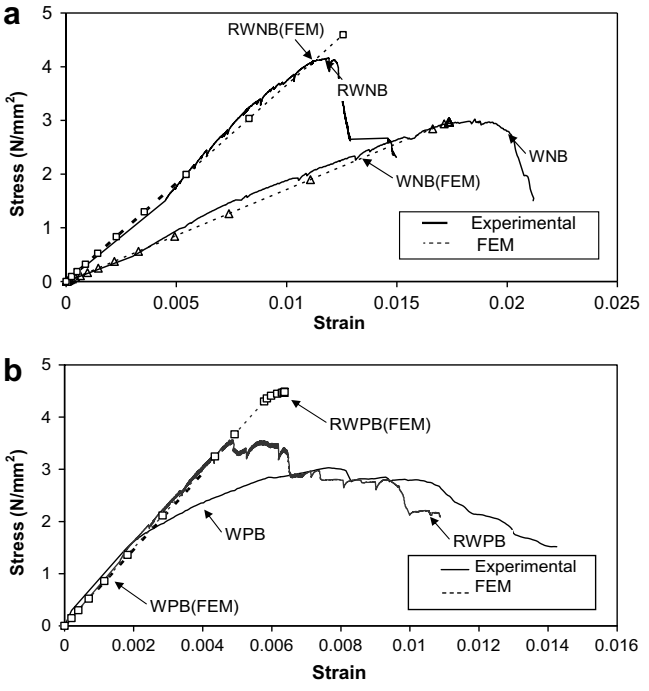

Fig. 8. Comparison of Fe result with experimental data for retrofitted wallettes under compression: (a) normal to bed joints and (b) parallel to bed joints.

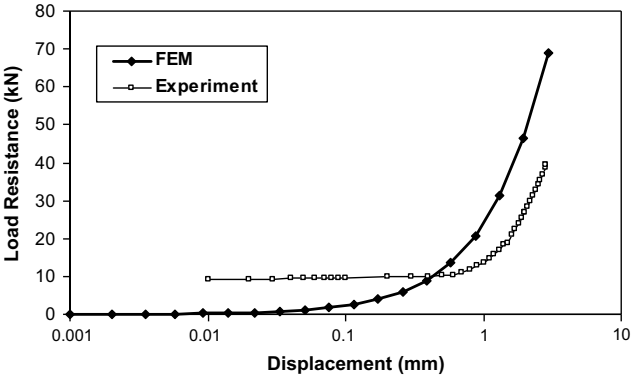

Fig. 9. Comparison of Fe results with experiment data.

3.5. Effect of orientation of fibers and thickness of GFRP composite

Parametric studies were also conducted to study the increase in load resistance of wallettes due to increase in the thickness of GFRP composite wrapping and change in the orientation of fibers. The material orientation of

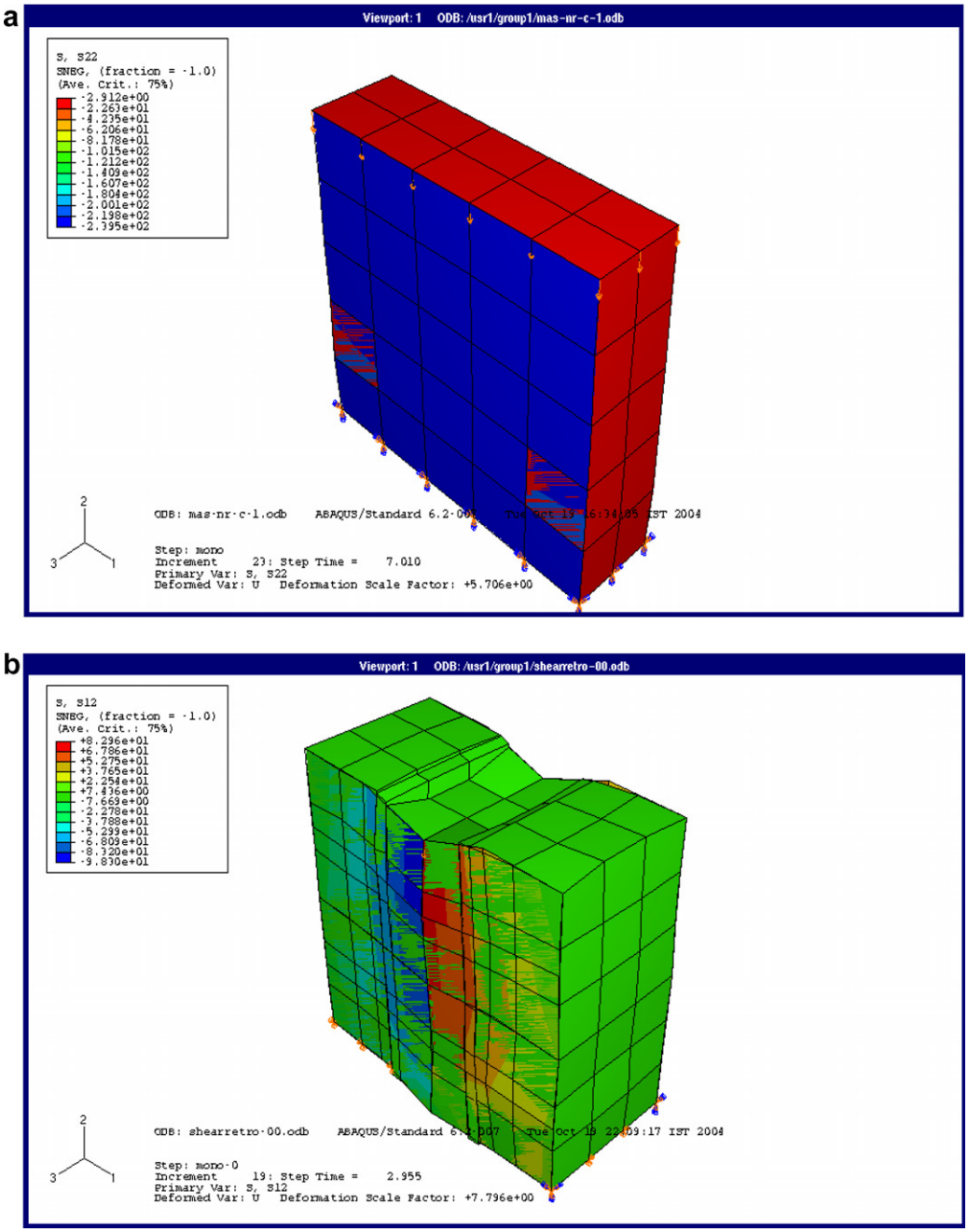

Fig. 10. Stress distribution: (a) compressive stress on wallette and (b) shear stress on the triplet.

GFRP composite was defined by representing the warp and weft directions of the fibers in the shell element. The local axes of material orientation follow the curvature of the modeled surface. Specifically, the local axes remain normal to the shell surface. Since, there was perfect bond assumed to exist at the interface between the GFRP composite and the masonry surface, the strains experienced by the GFRP composite at the middle of the wallette were relatively low compared to the strains obtained from experiments. Due to that the results of the finite element model were compared with the experimental data up to the ultimate deformation obtained from experiments. The finite element analysis was carried up to the experimental ultimate deformation of 4.9 mm for the wallettes. The load resistance and stiffness of the retrofitted wallettes was increased with the increase in the thickness of GFRP composite (Fig. 11a). Minor change in the load resistance and stiffness was observed with the change in the orientation of fiber direction (Fig. 11b). This is due to the fact that the material properties obtained for the orthotropic GFRP material were nearly the same ($E_x = 12{,}986$ N/mm^2 and $E_y = 11{,}500$ N/mm^2). It should also be noted that rovings were not used for retrofitting. Woven roving mat with nearly the same weight fraction of fibers in the

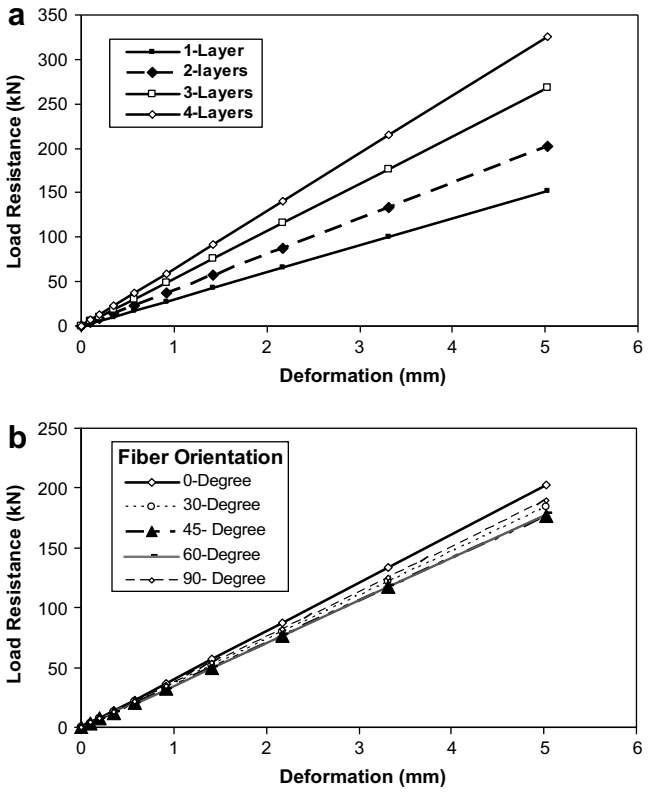

Fig. 11. Effect of: (a) number of layers and (b) orientation of fibers on the behaviour of masonry wallettes under compression.

warp and weft directions was used. Accordingly, the strength and stiffness of the GFRP composite was also almost same in the warp and weft direction. However, if different material properties are given in the warp and weft directions considerably then there will be a change in the load resistance. Parametric studies were also conducted to study the increase in load resistance of shear triplets by increasing the thickness of GFRP wrapping and by changing the orientation of fibers such as 0°, 30°, 45°, 60°, 90°, respectively. Since there was perfect bond at the interface between the GFRP and masonry surface, the strains experienced by GFRP was relatively low compared to the strains observed from experiments. Due to that the results from the finite element analysis were compared with the experimental data up to the ultimate deformation of 3.0 mm observed in the testing of triplets. The load resistance increased linearly with increase in the thickness of GFRP composite up to 5 kN for every additional layer (Fig. 12a). It is interesting to note that the deformation capacity is not increased with increase in the thickness of GFRP composites. Since the material properties adopted for the orthotropic GFRP material were nearly the same as $E_x = 12{,}986\ \mathrm{N/mm^2}$ and $E_y = 11{,}500\ \mathrm{N/mm^2}$ there was no appreciable change in the load resistance with respect to change in the orientation of fibers (Fig. 12b). Only minor change was observed due to the fact that weight fraction of fibers were almost the same in warp and weft directions. However, if different

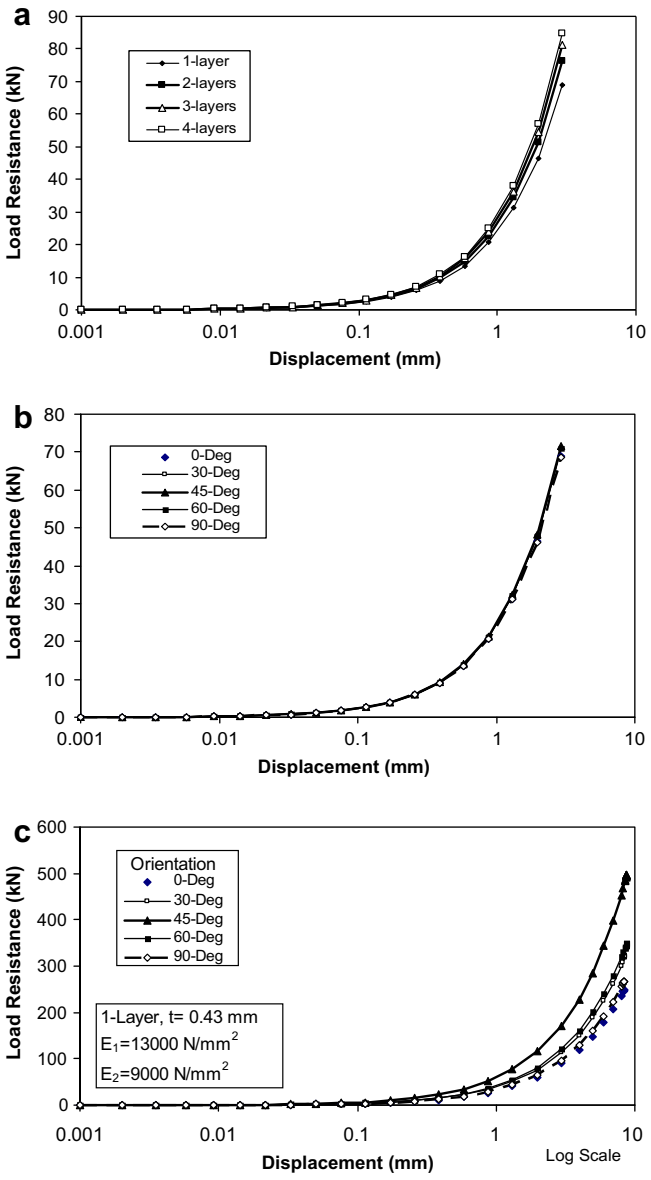

Fig. 12. Effect of: (a) number of layers, (b) orientation of fibers and (c) orientation of fibers with modified properties on the behaviour of masonry shear triplets under shear.

material properties are given in the warp and weft directions considerably, there will be a change in the load resistance (Fig. 12c).

4. Discussion of results

The experimental results showed that the modulus of brick was up to 52% of the mortar used and this is different from the brick masonry structures in North America, Europe and Canada where the bricks have higher modulus compared to mortar. The combination of strong mortar and weak brick leads to an unfavorable situation under compression producing lateral tensile stresses in mortar and triaxial compressive stresses in brick resulting in brittle failure of wallettes. This can

be taken into account in the analysis and design of load bearing masonry structures by adopting suitable reduction factors in the calculations of modulus of elasticity of masonry. Experimental results showed that the load resistance of masonry wallettes and triplets was increased due to retrofitting using GFRP composites. The failure strain of the wallette reduced from 0.0189 to 0.0115 under compression normal to bed joints and it reduced from 0.00771 to 0.00570 under compression parallel to bed joint. The strain in the GFRP laminate at the failure load of wallettes was found to be very much lower than the failure strain observed from the coupon tension tests. The failure mode of the GFRP retrofitted wallettes was through compression failure of masonry under axial compression. In the case of shear triplets, GFRP retrofitting increased the strength and deformational capacity. The increase in the ultimate shear deformation was from 0.018 mm to 2.967 mm. The shear triplet failed by cracking of middle brick though there was initial local debonding along the bed joint mortar. However, the overall bond between the GFRP laminate and triplet surface was intact up to failure. This shows that the GFRP retrofitting can significantly enhance the seismic performance of the masonry walls under shear, since the forces generated in the earthquake are predominantly shear. The major source of injury during earthquakes will be prevented due to GFRP retrofitting with proper anchorage at the ends by the holding of debris of masonry even after failure. In case of retrofitting of masonry load bearing walls with GFRP composites, the thickness (number of layers) of GFRP fabric/sheets needs to be optimized for the effective utilization. Only limited numbers of specimens are tested under compression and shear in this study. These test results should be further confirmed by large experimental program that also takes in to account different types of masonry and FRP types and configurations. Moreover, masonry structures are sensitive to scale and size effect. The dimensions of the wallettes and another related to the ratio between the unit dimension of brick and nominal dimension of the wallettes plays an important role on strength and stiffness characteristics of masonry assemblages. More number of configurations with different orientations also needs to be tested to validate the current code standards for masonry made with low stiffness bricks and high stiffness mortar.

The finite element model results correlated with the experimental data for the control and GFRP retrofitted wallette specimens up to the elastic limit reasonably well considering the inherent variation in materials properties of masonry. The numerical analyses provided useful insight into phenomena that are virtually impossible to observe experimentally. The increase in the ultimate strength from finite element study was up to 48% and 21% compared to the experimental increase of 20% and 5% for the wallettes under compression normal to bed joints and parallel to bed joints respectively due to GFRP retrofitting. The difference in the predictions of FE models is due to the macromodeling strategy adopted and perfect bond assumption neglecting local debonding failures. The increase in the secant stiffness of wallettes at failure from the finite element study was up to 115% and 15% compared to experimental increase of 110% and 43% under compression normal to bed joints and parallel to bed joints respectively due to GFRP retrofitting. Both the experimental and FE results proved that retrofitting of wallettes using GFRP composites increased the strength and stiffness of wallettes. The comparison of FE results with experiments showed that the macromodel can be used to study the behaviour of masonry wallettes reasonably well considering the advantages of macromodeling owing to its simplicity and reduction in computational cost. The FE results of micromodeling of shear triplet showed that the interfacial shear stress concentrations between the brick and mortar surfaces were reduced due to retrofitting with GFRP composites. The micromodel of shear triplet over predicted the stiffness and strength of experimental data and is mainly due to the perfect bond assumption between the triplet surface and GFRP composite neglecting local debonding along the bed joint mortar. The bond between GFRP composite and masonry substrate plays an important role in predicting the behaviour of GFRP composite retrofitted wallettes and triplets. Further experiments are needed to study the interface characteristics between the GFRP composite and masonry surface to model the bond accurately in FE study for better predictions. The FE results of masonry wallettes and triplets showed that the stiffness and load resistance of GFRP retrofitted wallettes and triplets increased linearly with increase in thickness of GFRP composites. There was no appreciable change in the ultimate load resistance with change in the orientation of fibers since orthotropic properties for the GFRP composite were almost same due to same amount of weight fraction of fibers.

5. Summary and conclusions

The material characterization of brick masonry made with low stiffness brick and high stiffness mortar and GFRP composites was carried out by casting nine wallettes, three shear triplets and coupons cut from GFRP composites. Six wallettes and three shear triplet specimens were retrofitted with GFRP composites. The behaviour of masonry wallettes retrofitted with GFRP composites under compression normal to bed joints, parallel to the bed joints and their failure modes were studied and compared with the control specimens. The behaviour of GFRP retrofitted shear triplets was studied and compared to that of control shear triplets for increase in the load resistance and deformational capacity. Finite element models for the analysis of wallettes and shear triplets was developed using the FE software ABAQUS and validated with the experimental data.

The FE models were calibrated based on the behaviour of control specimens. The concepts of macromodeling with smeared crack concrete model for masonry wallettes and micromodeling with the elastic properties of brick and mortar for shear triplets were used for the analysis. Comparison of results proved that the FE models were able to predict the load carrying capacity of FRP retrofitted masonry wallettes and shear triplets reasonably well. The effect of varying the thickness and change in the orientation of fibers of GFRP composite on the behaviour of retrofitted wallettes and triplets were also studied. The results have proved that GFRP composite can enhance the shear and compressive strength of unreinforced masonry. The study has demonstrated that reliable numerical models represent very valuable tools for gaining insight into phenomena that are extremely difficult to assess experimentally. Based on this study the following major conclusions are drawn.

(i) Brick masonry constructed with high stiffness cement mortar and low stiffness bricks leads to development of lateral tensile stresses in mortar leading to early cracking of mortar thereby resulting in the brittle failure of wallettes under compression.
(ii) The strength of masonry wallettes under compression normal and parallel to bed joint is increased up to 20% and 5%, respectively due to GFRP composite retrofitting.
(iii) The axial stiffness of masonry wallettes under compression normal and parallel to bed joint is increased up to 110% and 43%, respectively due to GFRP composite retrofitting.
(iv) The strength and deformational capacity of shear triplets under shear are increased due to GFRP composite retrofitting and the increase in the shear strength is about 180%.
(v) GFRP composite retrofitting helps to prevent the mortar deterioration by weathering, shrinkage and drying and improves the durability of masonry structures.
(vi) Smeared crack concrete model can be used to predict the behaviour of masonry wallettes under monotonic loading and micromodeling is feasible for the analysis of shear triplets.
(vii) The interfacial shear stress concentrations between the brick and mortar surfaces are reduced due to retrofitting of shear triplets with GFRP composites. The GFRP retrofitting also reduces the anisotropic nature of masonry.
(viii) Further experiments are needed to study the interface characteristics between the GFRP composite and masonry surface to model bond in the FE study for better predictions. Optimization of FRP retrofitting configurations for the desired failure modes is also a scope for further study using macro and micro modeling.

References

[1] Al-Salloum YA, Almusallam TH. Load capacity of concrete masonry block walls strengthened with epoxy-bonded GFRP sheets. J Compos Mater 2005;39(24):2243–8.
[2] Andreaus U. Failure criteria for masonry panels under in-plane loading. J Struct Eng 1996;122(1):37–46.
[3] Ascione L, Feo L, Fraternali F. Load carrying capacity of 2D FRP/strengthened masonry structures. J Compos, Part B: Eng 2005:1–8.
[4] Berman JB, Al-Chaar GK, Dutta PK. Biaxial loading and failure behavior of brick triplets with fiber-reinforced polymer composite upgrades. Technical Report, 13 December 2002, USA CERL, Champaign, IL. Report Number ERDC/ERL TR-02-7.
[5] BS 2782-10: Method 1006. Methods of testing plastics, glass reinforced plastics: determination of tensile properties; 1996.
[6] Dhanasekar M, Page AW, Kleeman PW. The failure of brick masonry under biaxial stresses. Proc Inst Civil Engrs (Part 2) 1985;79:295–313.
[7] Ehsani MR, Saadatmanesh H, Al-Saidy A. Shear behaviour of URM retrofitted with FRP overlays. J Compos Construct ASCE 1997;1(1):17–25.
[8] Ehsani MR, Saadatmanesh H, Velazquez-Dimas JI. Behavior of retrofitted URM walls under simulated earthquake loading. ASCE J Compos Construct 1999;3(3):134–42.
[9] El-Dakhakhni WW, Hamid AA, Hakam ZHR, Elgaaly M. Hazard mitigation and strengthening of unreinforced masonry walls using composites. J Compos Struct 2006;71(4):458–77.
[10] El-Sakhawy NR, Raof HA, Gouhar A. Shearing behavior of joints in load-bearing masonry wall. J Mater Civil Eng 2002;14(2):145–50.
[11] EN 1052-1. Methods of test for masonry – Part 1: determination of compressive strength 1998, European Standards.
[12] Eusebio M, Palumbo P, Lozza F, Manfredi G. Numerical modeling of masonry panels strengthened using FRPs. Proceedings of Finite Element in Civil Engineering Applications; 2002. p. 295–303. ISBN: 90 5809 530 4.
[13] FEMA306. Evaluation of earthquake damaged concrete and masonry wall buildings-basic procedures. Technical report, Federal Emergency Management Agency (FEMA), FEMA 306, Prepared by Applied Technology Council; 1999.
[14] Gabor A, Bennani A, Jacquelyn E, Lebon F. Modelling approaches of the in-plane shear behaviour of unreinforced and FRP strengthened masonry panels. J Compos Struct 2006;74(3):277–88.
[15] Giordano A, Mele E, De Luca A. Modeling of historical masonry structures: comparison of different approaches through a case study. Eng Struct J 2002;24:1057–69.
[16] Gumaste. Studies on strength and elasticity of brick masonry walls. PhD thesis 2004, Department of Civil Engineering, IISc, Bangalore, India.
[17] Hamid AA, El-Dakhakhni WW, Hakam ZHR, Elgaaly M. Behavior of composite unreinforced masonry-fiber reinforced polymer wall assemblages under in-plane loading. J Compos Construct 2005;9(1):73–83.
[18] Hibbit D, Karlson B, Sorensen P. ABAQUS/Standard theory manual. HKS; 2002.
[19] IS: 3495. Specification for methods of tests for burnt clay building brick. Bureau of Indian Standards, New Delhi, 1992.
[20] IS: 1905. Indian standard code of practice for structural use of unreinforced masonry. Bureau of Indian Standards, New Delhi; 1987.
[21] Lee J, Pande G, Midelton J, Kralj B. Numerical modeling of brick masonry panels subject to lateral loadings. Comput Struct 1996;61(4):735–45.
[22] Lofti HR, Shing PB. An appraisal of smeared crack models for masonry shear wall analysis. Comput Struct 1991;41(3):413–25.
[23] Lourenco PB. Computational strategies for masonry structures. PhD thesis, TU-Delft; 1996, ISBN 90-407-1221-2.

[24] Luciano R, Sacco E. Damage of masonry panels reinforced by FRP sheets. Int J Solids Struct 1998;35(15):1723–41.
[25] Marifia S, Sacco E. Modeling of reinforced masonry elements. Int J Solids Struct 2001;38:4177–98.
[26] Page AW. Finite element model for masonry. J Struct Div 1978;104(8):1267–85.
[27] Sahlin S. Structural masonry. New Jersey: Prentice-Hall; 1971.
[28] Shrive NG, Masia MJ, Lissel SL. Strengthening and rehabilitation using fiber reinforced polymers. In: Lourenco PB, Roca P, editors. Historical Constructions, Guimaraes; 2001.p. 1047–56.
[29] Triantafillou TC. Strengthening of masonry structures using epoxy-bonded FRP laminates. J Compos Construct 1998;2(2):96–104.
[30] Valluzi MR, Tinazzi D, Modena C. Shear behaviour of masonry panels strengthened by FRP laminates. J Construct Build Mater 2002;16:409–16.